J. Fluid Mech. (1985), *vol.* 156, *pp.* 23–38
Printed in Great Britain

Electrostatically enhanced film condensation

By F. M. JOOS AND R. W. L. SNADDON
General Electric Corporate Research and Development, Schenectady, New York 12301

(Received 10 February 1984 and in revised form 31 October 1984)

This paper presents a model for film-condensation heat transfer on a general cylindrical surface in the presence of a non-uniform electrostatic field. The steady-state liquid-film flow is assumed to be fully developed and smooth. The liquid is electrically non-conducting. The vapour in contact with the film is pure and saturated. We also describe two experiments in which R113 is condensed in a tube. In one case condensation occurs in an asymmetric electric field as described by the model. In the other case, done for comparison, it occurs in an axisymmetric one. We report average heat-transfer measurements and visual observations in both cases. Comparison of the theory with the first experiment is good, despite the model not accounting for the film's waviness.

1. Introduction

When an electrostatic field is imposed on a liquid, the liquid is subjected to electric stresses. These stresses depend on the distribution of free charge and spatial variations in the field and the dielectric constant. Across an interface the dielectric constant (and thus the electric field) usually changes abruptly, producing predominantly normal surface stresses that are higher than those within the liquid. Investigators have employed these stresses to enhance heat transfer. In the case of film condensation, electric fields have been used to decrease the film's heat-transfer resistance by thinning it. Choi (1968), Velkoff & Miller (1965), Didkovsky & Bologa (1981), Dyakowski, Trommelmans & Berghmans (1982) and Trommelmans & Berghmans (1982) have enhanced heat transfer by imposing a large field perpendicular to the liquid's free surface, producing surface waves with very thin film thicknesses at the troughs. Alternatively, non-uniform electric fields can be applied, producing varying normal stresses along the vapour–liquid interface, which 'pull' the film to a side, thus concentrating the condensate over small regions of the heat-transfer surface and reducing film thickness over the remaining surface. Holmes & Chapman (1970) applied this idea to condensation on a horizontal plate. The film was subjected to an electric field that varied along the plate, putting the film into motion. More recently, Yabe, Kikuchi & Taketoni (1982) have applied non-uniform electric fields, which 'pull' the liquid's surface outwards in order to mechanically skim off part of the condensate.

In this paper we investigate the electrostatic enhancement of film-condensation heat transfer in the presence of a gravitational field. Condensation occurs in a tube, which may be inclined, and the electric field is made to vary along the condensate surface in a fashion similar to Holmes & Chapman's work. Except for comparison, we will not consider enhancement due to waviness or wave instabilities. A two-dimensional modified Nusselt condensation-film theory is proposed. Two experiments are described, both performed in a vertical condensation tube but with different field

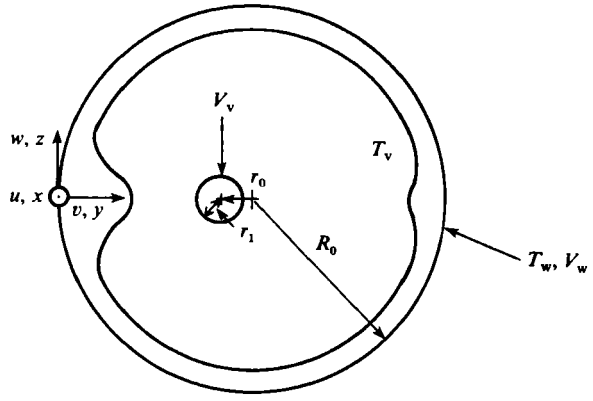

FIGURE 1. General configuration for the example calculation.

characteristics. In one we apply a field that pulls the film to a side; the other, used only for comparison, is very similar to Choi's, where the electric field is used to produce a wavy flow. The two mechanisms are discussed, and the results of the first experiment are compared with the predictions of the proposed film-thinning model.

2. Model

2.1. *Basic heat-transfer equations*

The physical model consists of a liquid film in contact with its saturated vapour on one side and a wall on the other. The wall is viewed as a segment of a general cylinder, which we will initially assume to have its line generators in the vertical x-direction. Figure 1 shows a particular case where the condensing wall is a circular cylinder. The liquid is subjected to body and interfacial stresses and the flow is assumed to be laminar, smooth and at steady state. Cartesian boundary-layer-type equations are valid when the film thickness is small compared with the wall dimensions (length, width and surface curvature). These are as follows:

mass

$$\frac{\partial u}{\partial x}+\frac{\partial v}{\partial y}+\frac{\partial w}{\partial z}=0; \tag{1}$$

momentum

in the vertical x-direction

$$0=-\frac{1}{\rho}\frac{\partial p}{\partial x}+\frac{f_{ex}}{\rho}+\frac{\rho-\rho_v}{\rho}g+\nu\frac{\partial^2 u}{\partial y^2}; \tag{2}$$

in the normal y-direction

$$0=-\frac{1}{\rho}\frac{\partial p}{\partial y}+\frac{f_{ey}}{\rho}; \tag{3}$$

in the tangential z-direction

$$0=-\frac{1}{\rho}\frac{\partial p}{\partial z}+\frac{f_{ez}}{\rho}+\nu\frac{\partial^2 w}{\partial y^2}; \tag{4}$$

and energy

$$0=\frac{k}{\rho c_p}\frac{\partial^2 T}{\partial y^2}; \tag{5}$$

here f_e represents the applied electric body force per unit volume. Equations (2)–(5) are steady-state equations for a thin liquid film. The convective terms were neglected in (2)–(4) because of the assumption that the film is fully developed. The error in neglecting convective terms in (5) is discussed by Rohsenow (1956).

Boundary conditions at the wall ($y = 0$) are

$$u = v = w = 0, \quad T = T_w. \tag{6}$$

At the free surface we assume that the vapour exerts no shear stress on the liquid. We require that the vapour is at the saturation temperature T_v. Thus at the liquid–vapour interface ($y = \delta$)

$$\frac{\partial u}{\partial y} = \frac{\partial w}{\partial y} = 0, \quad T = T_v. \tag{7}$$

Mass and energy balances at the interface yield

$$m = \rho u|_\delta \frac{\partial \delta}{\partial x} + \rho w|_\delta \frac{\partial \delta}{\partial z} - \rho v|_\delta, \tag{8}$$

$$m h_{fg} = -k \frac{\partial T}{\partial y}\bigg|_\delta. \tag{9}$$

Here m is the local mass-condensation rate per unit area. There exists a pressure condition at the interface due to the electrical field, which we will discuss later. In addition, we must impose an initial film thickness

$$\delta = \delta_0(z) \quad \text{at } x = x_0. \tag{10}$$

Our earlier assumptions that the wall had small curvature and the film was smooth allow us to disregard surface-tension effects.

2.2. *Basic electrostatic equations*

In the absence of any net free charge, the electrostatically body forces in the liquid are given by the following expression, which can be found in the texts by Landau & Lifshitz (1960) or Panofsky & Phillips (1962):

$$f_e = -\tfrac{1}{2}E^2 \nabla\epsilon + \nabla\left[\tfrac{1}{2}\rho\left(\frac{\partial\epsilon}{\partial\rho}\right)_T E^2\right], \tag{11a}$$

or equivalently

$$f_e = -\tfrac{1}{2}E^2\left(\frac{\partial\epsilon}{\partial T}\right)_\rho \nabla T + \tfrac{1}{2}\rho\,\nabla\left[\left(\frac{\partial\epsilon}{\partial\rho}\right)_T E^2\right]. \tag{11b}$$

The surface stresses are normal to the interface and produce a pressure difference across it:

$$p|_\delta - p_v = \left\{\frac{\rho E^2}{2}\left(\frac{\partial\epsilon}{\partial\rho}\right)_T - \rho_v\left[\left(\frac{\epsilon}{\epsilon_v}\right)^2 E_n^2 + E_t^2\right]\left(\frac{\partial\epsilon_v}{\partial\rho_v}\right)_T - \tfrac{1}{2}(\epsilon - \epsilon_v)\left(\frac{\epsilon}{\epsilon_v}E_n^2 + E_t^2\right)\right\}\bigg|_\delta, \tag{12}$$

where the field components are taken on the liquid side of the interface. In §2.3 we will show that, under certain conditions applicable to the thin films dealt with in this paper, the forces in (11) are small compared with those originating from (12). In the absence of net free charge, the electric field $\boldsymbol{E}$ is determined from the electrostatic equations

$$\nabla^2 V = 0, \tag{13a}$$

where

$$\boldsymbol{E} = -\nabla V. \tag{13b}$$

(A)	$\frac{\tau_l}{\tau_e} = \frac{L}{u}\frac{\sigma}{\epsilon} \ll 1$ (d.c.) or $\sim \frac{\sigma}{\epsilon\omega} \ll 1$ (a.c.)
(B)	$\left(\frac{E_t}{E_n}\right)^2 \ll 1$
(C)	$\frac{\left(\frac{\epsilon}{\epsilon_v}\right)\left(\frac{\partial \epsilon_v}{\partial \rho_v}\right)_T \rho_v}{\epsilon - \epsilon_v} \ll 1$
(D)	$\frac{\frac{\partial}{\partial x}\int_0^\delta E^2\left(\frac{\partial \epsilon}{\partial T}\right)_\rho \frac{\partial T}{\partial y}\mathrm{d}y}{(\rho-\rho_v)g} \sim \frac{E_n^2\left(\frac{\partial \epsilon}{\partial T}\right)_\rho (T_v - T_w)}{(\rho-\rho_v)gL} \ll 1$
(E)	$\frac{\frac{\partial}{\partial x}\left[(\epsilon-\epsilon_v)\frac{\epsilon}{\epsilon_v}E_n^2\vert_\delta\right]}{(\rho-\rho_v)g} \sim \frac{(\epsilon-\epsilon_v)\frac{\epsilon}{\epsilon_v}E_n^2}{(\rho-\rho_v)gL} \ll 1$
(F)	$\frac{\frac{\partial}{\partial z}\int_0^\delta E^2\left(\frac{\partial \epsilon}{\partial T}\right)_\rho \frac{\partial T}{\partial y}\mathrm{d}y}{\frac{\partial}{\partial z}\left[(\epsilon-\epsilon_v)\frac{\epsilon}{\epsilon_v}E_n^2\vert_\delta\right]} \sim \frac{\left(\frac{\partial \epsilon}{\partial T}\right)_\rho (T_v - T_w)}{(\epsilon-\epsilon_v)\frac{\epsilon}{\epsilon_v}} \ll 1$

TABLE 1. Assumptions on the electrical terms

One electrode is the wall's surface, the other some surface in the vapour. Thus the boundary conditions are

$$V = V_w \quad \text{at } y = 0, \tag{14a}$$

$$V = V_v \quad \text{at surface } S_v \text{ in the vapour.} \tag{14b}$$

We must require that the potential V, the tangential component of the electric field E_t and the normal component of the electric induction ϵE_n be continuous at the liquid–vapour interface. The electric-field solution is thus coupled to the heat-transfer solution. However, in our development we will first assume that the field has already been established. Although our mathematical description of the electric-field effects assumes zero net free charge, in d.c. systems free charges can arise in the bulk and at interfaces owing to charge-injection or charge-separation phenomena, which are usually difficult to control. In addition to experimental verification, a charge-relaxation-time argument suggested by Jones (1978) substantiates the claim that even under d.c. conditions net free-charge (space-charge) effects can be neglected in the experimental system investigated in this paper.

2.3. *Reduction of the equations*

By combining (1), (6) and (8) we obtain an integral form of the mass-conservation equation:

$$m = \rho\frac{\partial}{\partial x}\int_0^\delta u\,\mathrm{d}y + \rho\frac{\partial}{\partial z}\int_0^\delta w\,\mathrm{d}y. \tag{15}$$

In table 1 we list assumptions made to reduce the electrical-field components in the momentum equations. In table 2, these assumptions are confirmed for the experimental example we present later. With the possible exception of condition A, the

Evaluation of assumptions		Estimated property values	
(A)	$\tau_l/\tau_e \approx 1.5\times10^{-2}$ (d.c.) or 8×10^{-5} (a.c.)	$\rho \approx 1.5\times10^{3}$ kg/m^3†	$\rho_v \approx 8$ kg/m^3†
(B)	$(E_t/E_n)^2 \approx 4\times10^{-4}$	$\epsilon_0 = 8.845\times10^{-12}$ F/m	$\epsilon/\epsilon_0 = 2.41$
(C)	$\dfrac{\dfrac{\epsilon}{\epsilon_v}\left(\dfrac{\partial\epsilon_v}{\partial\rho_v}\right)_T \rho_v}{\epsilon-\epsilon_v} \approx 0.02$	$\left(\dfrac{\partial(\epsilon/\epsilon_0)}{\partial T}\right)_\rho \approx -2\times10^{-3}$ K^{-1}†	$\epsilon_v/\epsilon_0 \approx 1.00$‡
		$\rho_v\left(\dfrac{\partial(\epsilon_v/\epsilon_0)}{\partial\rho_v}\right)_T \approx 0.0111$	$\sigma \approx 10^{-13}\,\Omega^{-1}$ m^{-1}
(D)	$\dfrac{E_n^2\left(\dfrac{\partial\epsilon}{\partial T}\right)_\rho (T_v-T_w)}{(\rho-\rho_v)gL} \approx 2\times10^{-4}$	$E_n \approx 2\times10^{6}$ V/m†	$g = 9.81$ m/s^2
		$E_t \approx 4\times10^{4}$ V/m†	$L = 0.69$ m
(E)	$\dfrac{(\epsilon-\epsilon_v)\dfrac{\epsilon}{\epsilon_v}E_n^2}{(\rho-\rho_v)gL} \approx 0.01$	$T_v-T_w \approx 30$ K†	$\delta \approx 0.2$ mm†
		$u \sim 0.2$ m/s†	$R_0 = 9.6$ mm
		$\omega = 60$ Hz	
(F)	$\dfrac{\left(\dfrac{\partial\epsilon}{\partial T}\right)_\rho (T_v-T_w)}{(\epsilon-\epsilon_v)\epsilon/\epsilon_v} \approx 0.02$		

† Typical value.
‡ No value was found in the literature; a typical value of similar substance used instead.
‖ Calculated using the Clausius–Mossotti relation.

TABLE 2

assumptions should be valid in other setups where the film is thin and the liquid is being pulled to a side by electric fields (as opposed to becoming wavy). The pressure is determined by integrating (3), combining it with (11) and (12), and applying assumptions B and C of table 1:

$$p = p_v + \tfrac{1}{2}\rho\left(\frac{\partial\epsilon}{\partial\rho}\right)_T E^2|_\delta - \tfrac{1}{2}(\epsilon-\epsilon_v)\frac{\epsilon}{\epsilon_v}E_n^2|_\delta + \frac{1}{2}\int_y^\delta E^2\left(\frac{\partial\epsilon}{\partial T}\right)_\rho \frac{\partial T}{\partial y}\,\mathrm{d}y. \tag{16}$$

Substituting (11) and (16) in (2) and (4) and applying assumptions D and E, and F, respectively, yields

$$\frac{\partial^2 u}{\partial y^2} = -\frac{\rho-\rho_v}{\rho\nu}g, \tag{17}$$

$$\frac{\partial^2 w}{\partial y^2} = -\frac{1}{2\rho\nu}\frac{\partial}{\partial z}\left[(\epsilon-\epsilon_v)\frac{\epsilon}{\epsilon_v}E_n^2|_\delta\right]. \tag{18}$$

Integrating (5), (17) and (18) and applying the boundary conditions (6), (7) and (9) yields

$$\frac{k}{\delta}(T_v-T_w) = m h_{fg}, \tag{19}$$

$$u = \frac{\rho-\rho_v}{\rho\nu}g[\delta-\tfrac{1}{2}y]\,y, \tag{20}$$

$$w = \frac{1}{2\rho\nu}\frac{\partial}{\partial z}\left[(\epsilon-\epsilon_v)\frac{\epsilon}{\epsilon_v}E_n^2|_\delta\right](\delta-\tfrac{1}{2}y)\,y. \tag{21}$$

Combining (15) and (19)–(21) to eliminate u, w and m, we obtain a differential equation for δ^4:

$$\frac{\partial f}{\partial x}+\psi\frac{\partial f}{\partial z}+\frac{4}{3}\frac{\partial \psi}{\partial z}f=\gamma, \tag{22a}$$

where

$$\psi=\frac{1}{2(\rho-\rho_v)g}\frac{\partial}{\partial z}\left[(\epsilon-\epsilon_v)\frac{\epsilon}{\epsilon_v}E_n^2|_\delta\right], \tag{22b}$$

$$\gamma=\frac{4k\nu(T_v-T_w)}{(\rho-\rho_v)gh_{fg}} \tag{22c}$$

and

$$f=\delta^4. \tag{22d}$$

2.4. *Solution*

In general T_w and E_n will vary both in the x- and z-directions. We will first assume that they only vary in the z-direction. the solution of (22) is obtained by first making the changes of variables

$$t=\int_\alpha^z\frac{dz}{\psi},\quad s=x-\int_\alpha^z\frac{dz}{\psi}, \tag{23}$$

which reduce the differential equation to a first-order ordinary differential equation that is readily solved:

$$f(x,z)=\frac{\operatorname{sgn}(\psi)}{|\psi|^{\frac{4}{3}}}\int_{z^0}^z\gamma|\psi|^{\frac{1}{3}}dz+\left|\frac{\psi(z^0)}{\psi(z)}\right|^{\frac{4}{3}}f_0(z^0), \tag{24a}$$

where z^0 is determined from

$$x-x_0=\int_{z^0}^z\frac{dz}{\psi}. \tag{24b}$$

$f_0(z)=f(x_0,z)$ is the initial condition taken at $x=x_0$ (see (10)) and sgn is the sign function.

A useful particular case is that when the wall temperature is constant and the inlet is dry, i.e. $f_0(z)=f(0,z)=0$; the solution can then be divided by the Nusselt (zero-field) film thickness δ_{Nu}, to give a normalized film thickness

$$\frac{\delta(x,z)}{\delta_{Nu}(x)}=\frac{1}{|\psi|^{\frac{1}{3}}}\left[\frac{\operatorname{sgn}(\psi)}{x}\int_{z^0}^z|\psi|^{\frac{1}{3}}dz\right]^{\frac{1}{4}}. \tag{25}$$

Notice that this equation is independent of γ; hence it is independent of the liquid's viscosity, latent heat and thermal conductivity and the driving temperature difference.

The solution of (22) when ψ and γ (i.e. E_n and T_w) vary in the x-direction is obtained from (25). Assuming first $\psi(x,z)$ and $\gamma(x,z)$ are piecewise-constant in x, we define

$$\psi_i(z)=\psi(x,z),\quad \gamma_i(z)=\gamma(x,z)\quad \text{for some } x_i<x<x_{i+1}. \tag{26}$$

Then by induction one can prove that

$$f_n(x_n,z_0^n)=\frac{1}{|\psi_{n-1}(z_0^n)|^{\frac{4}{3}}}\sum_{i=0}^{n-1}\left\{\int_{z_{n-i}^i}^{z_{n-i-1}^{i+1}}\gamma_i|\psi_i|^{\frac{1}{3}}\operatorname{sgn}(\psi_i)\,dz\left|\prod_{j=i+1}^{n-1}\frac{\psi_j(z_{n-j}^j)}{\psi_{j-1}(z_{n-j}^j)}\right|^{\frac{4}{3}}\right\}$$
$$+\left|\prod_{i=1}^{n-1}\frac{\psi_i(z_{n-1}^i)}{\psi_{i-1}(z_{n-1}^i)}\right|^{\frac{4}{3}}\left|\frac{\psi_0(z_n^0)}{\psi_{n-1}(z_0^n)}\right|^{\frac{4}{3}}f(x_0,z_n^0), \tag{27a}$$

where
$$x_{i+1}-x_i = \int_{z_{n-i}^i}^{z_{n-i-1}^{i+1}} \frac{\mathrm{d}z}{\psi_i}, \tag{27b}$$

and x_n and z_0^n are the independent variables. By demanding that

$$z_0^n = z, \quad \Delta x = x_{i+1}-x_i, \quad n\Delta x = x-x_0, \quad n\to\infty, \tag{28}$$

we find the solution to (22) with continuously varying coefficients:

$$f(x,z) = \frac{1}{|\psi(x,z)|^{\frac{4}{3}}}\int_{x_0}^{x}\left\{\gamma(x',z^*(x'))\,|\psi(x',z^*(x'))|^{\frac{4}{3}} \times \exp\left[\frac{4}{3}\int_{x'}^{x}\frac{\partial}{\partial x''}\ln|\psi(x'',z^*(x''))|\,\mathrm{d}x''\right]\right\}\mathrm{d}x' + \left[\frac{\psi(x_0,z^*(x_0))}{\psi(x,z)}\right]^{\frac{4}{3}}\exp\left[\frac{4}{3}\int_{x_0}^{x}\frac{\partial}{\partial x'}\ln|\psi(x',z^*(x'))|\,\mathrm{d}x'\right]f(x_0,z^*(x_0)), \tag{29}$$

where $z^*(x')$ is determined from

$$\frac{\partial z^*}{\partial x'} = \psi(x',z^*) \tag{30}$$

with boundary condition $z^*(x) = z$ and where $f(x_0,z)$ is known. Once $f(x,z)$ is determined, the local heat-transfer coefficient is found from

$$h = \frac{k\left.\frac{\partial T}{\partial y}\right|_{\mathrm{w}}}{T_{\mathrm{v}}-T_{\mathrm{w}}}. \tag{31}$$

For simplicity we have assumed that the condensation wall was cylindrical with vertical generating lines. This condition makes the body force constant in the direction of the generating lines. We may relax this requirement to assume that the angle of the generating lines to the vertical is maintained constant. Then the development of (22)–(31) still holds, except that now (22*b*) becomes

$$\psi = \frac{1}{2(\rho-\rho_{\mathrm{v}})g_x}\frac{\partial}{\partial z}\left[(\epsilon-\epsilon_{\mathrm{v}})\frac{\epsilon}{\epsilon_{\mathrm{v}}}E_n^2|_\delta\right]+\frac{g_z}{g_x} \tag{32}$$

and g_x replaces g in (22*c*). Here g_z is a variable gravitational component in the z-direction, and g_x is its constant component in the x-direction, which still coincides with the generating lines.

2.5. *Electric-field correction*

The model we have presented assumes that the electric field has been pre-established, although the field is indeed coupled to the liquid-film distribution. Often, as is the case for our experiment, the liquid film is thin enough in the areas of interest to approximate the field strength adequately at the liquid–vapour interface by the magnitude it would have at the wall if the tube were dry, multiplied by the ratio of dielectric constants $\epsilon/\epsilon_{\mathrm{v}}$. However, if this first approximation was not sufficient, then a relaxation technique could probably be used. The method would require calculating iteratively the liquid distribution assuming an interfacial field strength (initially, the field at the condensation wall in the dry-wall case) and then calculating a new electric field that accounted for the new liquid-film distribution.

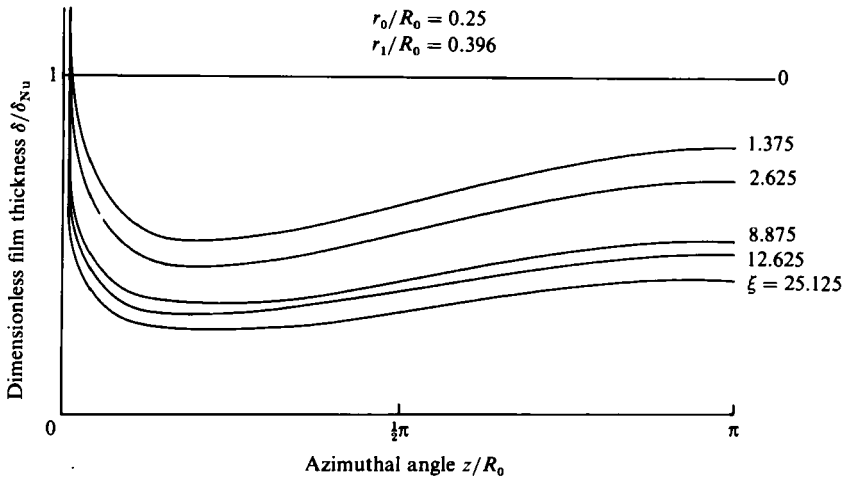

FIGURE 2. Calculated film thickness at the wall's surface, at different heights.

3. Example calculation

The theory was tested by an experiment that we describe in §4. Here we study the application of the theory to the experimental configuration. Consider two circular cylindrical electrodes (figure 1). The outer one serves as the condensation wall, which is at temperature T_w. The saturated vapour, at temperature T_v, is in contact with the inside of the tube. The inner electrode is placed eccentrically so that at any height there is an azimuthally changing electric field at the condensate's surface. The length of the outer electrode is much larger than its diameter. We approximate the electric field by that of the dry system. Because the cylindrical electrodes are long compared with the diameter of the largest one, (13) and (14) can be reduced to a two-dimensional Dirichlet problem with boundaries at two eccentric circles. The solution to this problem can be found in Churchill, Brown & Verhey (1974). The field at the wall is calculated, and then the electric surface-force parameter ψ is determined:

$$\psi = -\frac{\frac{\epsilon}{\epsilon_v}-1}{(\rho-\rho_v)g}\,\frac{\epsilon}{\epsilon/\epsilon_v}\,\frac{(V_v-V_w)^2}{(2R_0)^3}\,\frac{16a(a^2-1)^2}{(\ln R_1)^2(a^2+1)^3}\,\frac{\sin\frac{z}{R_0}}{\left[1-\frac{2a}{a^2+1}\cos\frac{z}{R_0}\right]^3}, \tag{33a}$$

where a and R_1 are the geometrical dimensionless parameters

$$a = \left\{1+\left(\frac{r_0}{R_0}\right)^2-\left(\frac{r_1}{R_0}\right)^2+\left[1-\left(\frac{r_0+r_1}{R_0}\right)^2\right]\left[1-\left(\frac{r_0-r_1}{R_0}\right)^2\right]^{\frac{1}{2}}\right\}\Big/\frac{2r_0}{R_0}, \tag{33b}$$

$$R_1 = \left\{1-\left(\frac{r_0}{R_0}\right)^2+\left(\frac{r_1}{R_0}\right)^2+\left[1-\left(\frac{r_0+r_1}{R_0}\right)^2\right]\left[1-\left(\frac{r_0-r_1}{R_0}\right)^2\right]^{\frac{1}{2}}\right\}\Big/\frac{2r_1}{R_0}. \tag{33c}$$

Figure 2 shows the calculated normalized film-thickness distribution along the wall, for different values of the dimensionless parameter ξ, which is essentially a simplified form of the force ratio ψ multiplied by the dimensionless length $x/2R_0$:

$$\xi = \frac{\epsilon/\epsilon_v-1}{\epsilon/\epsilon_v}\,\frac{\epsilon(V_v-V_w)^2x}{(2R_0)^4(\rho-\rho_v)g}. \tag{34}$$

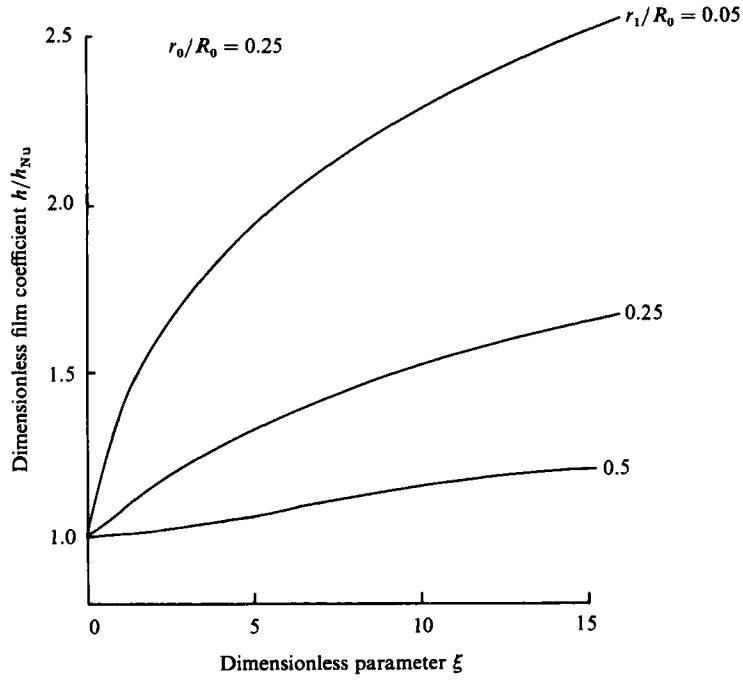

FIGURE 3. Calculated average heat-transfer coefficient for an electrode diameter ratio of 0.25 and different eccentricities.

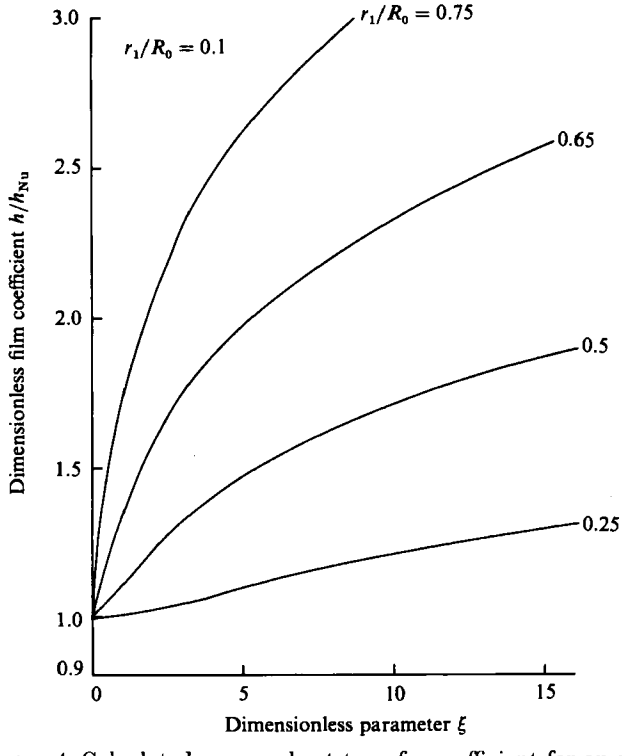

FIGURE 4. Calculated average heat-transfer coefficient for an electrode diameter ratio of 0.1 and different eccentricities.

As expected, the film's thickness is reduced significantly along most of the wall, but becomes much thicker where the field is strongest. This trend increases with distance from the inlet. The model loses validity earliest in the region where the film is thickest. It is here where the discrepancy of the electric field at the surface and at the dry wall will be greatest; cusped waves will form here first, and eventually the film will come into contact with the inner electrode. However, for the purposes of heat-transfer calculations this region is of the least interest, as the resistance is highest and represents only a small fraction of the surface, contributing minimally to the average film coefficient. We determine the average heat-transfer rate by integrating (31) over the surface of the condensation tube and dividing by its area. In figures 3 and 4 we present the average heat-transfer coefficient normalized by the average Nusselt heat-transfer coefficient as a function of the dimensionless parameter ξ for different inner electrode diameters and eccentricities. Of interest is the asymptotic behaviour of the heat-transfer coefficient for large values of ξ. In this case $z^0 \approx \pi R_0$ in (24*b*) for ψ given by (33*a*). Applying (25), the normalized film thickness is

$$\frac{\delta(x,z)}{\delta_{\mathrm{Nu}}(x)} \approx \frac{1}{2\xi^{\frac{1}{4}}}\left[\frac{(\ln R_1)^2(a^2+1)^3}{2a(a^2-1)^2}\right]^{\frac{1}{4}} \frac{1-\dfrac{2a}{a^2+1}\cos(z/R_0)}{\sin^{\frac{1}{3}}(z/R_0)}\left[\int_{z/R_0}^{\pi} \frac{\sin^{\frac{1}{3}}\theta\,\mathrm{d}\theta}{1-\dfrac{2a}{a^2+1}\cos\theta}\right]^{\frac{1}{4}}$$

$$\text{when } \frac{x}{R_0} \gg 1. \quad (35)$$

The ratio of the average heat-transfer coefficient to that corresponding to the zero-field vertical flat plate will be of the form

$$\frac{\bar{h}}{\bar{h}_{\mathrm{Nu}}} \sim \xi^{\frac{1}{4}} F(a, R_1) \quad \text{when } x/R_0 \gg 1. \quad (36)$$

Thus the heat-transfer advantage of establishing the electric field over the zero field case grows as the square root of the field strength and the fourth root of the length-to-diameter ratio.

4. Experiment, apparatus and procedure

Figure 5 is a diagram of the experimental apparatus. Refrigerant 113, the working fluid, is boiled in the heater. The vapour rises through the tube leading to the upper opening of the Pyrex-glass condensation tube. The condensation tube is water-cooled. The condensate is drawn down by gravity into a graduated separatory funnel and then back into the heater. The condensation tube's wall is 1.5 mm thick, with inner diameter 19.2 mm and length 690 mm; its inner surface is coated with a thin film of tin oxide, which is grounded. Inside this tube there is a second adjustable electrode consisting of a cylindrical rod 4.8 mm in diameter. The condensation tube is surrounded by a cooling water jacket consisting of an acrylic tube of outer diameter 64 mm and wall thickness 6.4 mm. The temperature of the cooling water could be varied; its flow rate was held at around 125×10^{-6} m^3/s. Inlet and outlet temperatures of the condensation tube and cooling jacket and the liquid temperature in the heater were measured with grounded thermocouples. Grounded pressure gauges were installed at the inlet and outlet of the condensation tube. There were two purge valves in the rig, situated at the inlet and outlet of the test section, and we operated the system at vapour pressures above atmospheric to ensure that the vapour was free

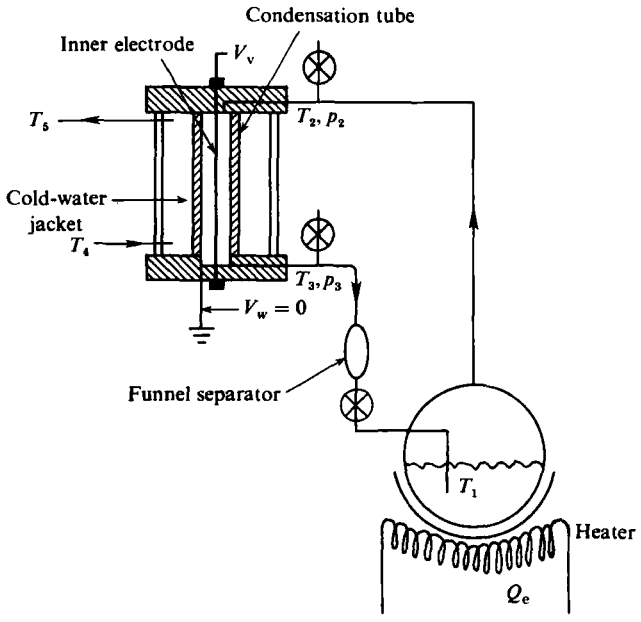

FIGURE 5. Schematic of the experimental apparatus.

of air. We assumed that there was no air in the system when the vapour temperature at the inlet and outlet of the test section differed by less than 0.3 °C. The pressure and temperature readings confirmed that we were operating very close to the saturation line. The condensation rate was measured by determining the time it took for 50×10^{-6} m^3 of condensate to enter the funnel separator. Four variables were controlled in this system: the heat-input rate (350–550 kWe), the cooling-water temperature (20–35 °C), the voltage drop between the electrodes (0–45 kV d.c. and 0–30 kV a.c.), and the position of the inner electrode (two positions were used: centred and 3.8 mm off-centre). Measurements of the variables were made for each set of conditions with the system in steady state.

Table 2 provides verification of the assumptions of the model, as described by the requirements in table 1, and estimates of the relevant properties we used to calculate the assumption. We obtained additional information on the condensate's properties and their variation with temperature from the manufacturer's literature.

5. Experimental results and comparison with theory

5.1. *Visual observations*

Visual observations were made of the flow characteristics of the condensate film, and, in the case of the eccentrically placed inner electrode, high-speed motion pictures of 250 frames per second were taken at three vertical locations and at voltages ranging from 0–45 kV. Figure 6 is a set of frames from the motion pictures taken halfway down the tube. For the flow-inlet and condensation-rate conditions examined some film waviness was present prior to the application of the field. With application of the field the condensate film did indeed thicken in the region where the inner electrode was closest to the tube's wall. At lower field strengths the amplitude of the waves in this region appeared to increase slightly and their group velocities increased,

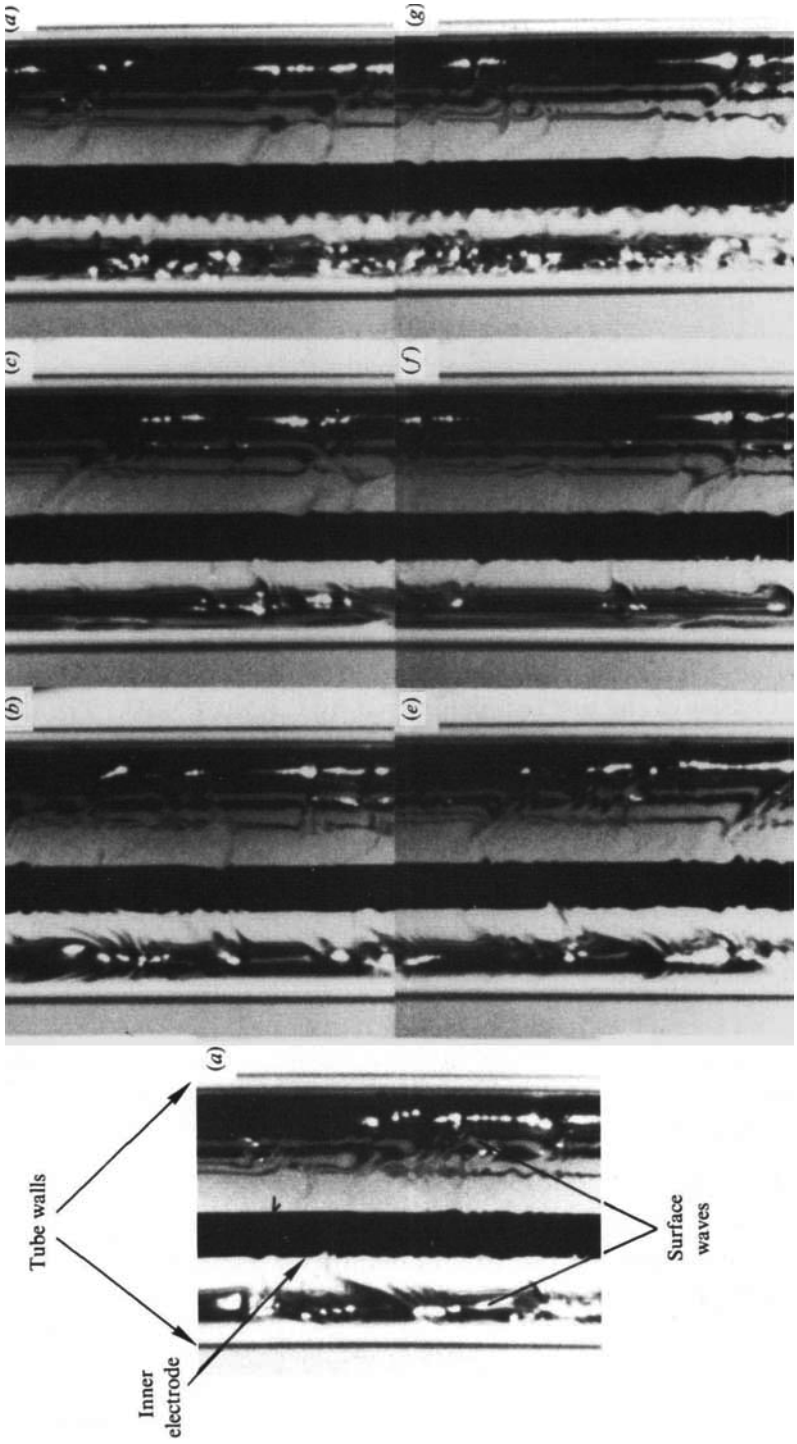

FIGURE 6. Frames from high-speed films 345 mm from condensation tube inlet with different applied fields: (*a*) 0 kV; (*b*) 5 kV (d.c.); (*c*) 15 kV (d.c.); (*d*) 25 kV (d.c.); (*e*) 5 kV (a.c.); (*f*)15 kV (a.c.); (*g*) 25 kV (a.c.); d.c. fields are of negative polarity.

consistent with the higher velocities expected from thicker films. As field strength was further increased, the surface of the faster-falling film flow closest to the inner electrode changed to a less-organized state comprising waves of smaller amplitude and shorter wavelength. At the highest field strengths the thinning action of the field was clearly evidenced by the paths of surface disturbances, which combined vertical motion with transverse motion towards the region of thickened film.

The cusped-wave instabilities reported by other workers appeared at about 17 kV. Although clearly visible on the inner electrode, they also appeared to be present on the tube-wall surface under some conditions. Their presence was confined to the region where the inner-electrode to wall gap was smallest. Even though such wave motions and instabilities were not included in the analysis, they are not expected to contribute significantly to changes in overall heat transfer, since their action was confined to the small region of the total heat-transfer surface where the thermal resistance is highest owing to the thicker film.

Careful scrutiny of the high-speed motion pictures indicated that the first appearance of waves on the inner electrode under moderate a.c. fields may have resulted from 60 Hz parametric instabilities, the apparent order and structure disappearing at higher field strengths. Apart from this, there were no other tangible differences between the film flows obtained with a.c. and d.c. excitation. This is in support of the earlier assertion that no net free charges were at work under d.c. conditions.

Visual observation of the concentric electrode arrangement also revealed the presence of waves prior to the application of the field. Here, however, the cusped waves were seen to appear at slightly higher voltages (20 kV), and they were evenly distributed over the inner-electrode and tube-wall surfaces.

With the exception of the cusped instabilities found at the higher voltages in the thicker-film region, the amplitude of the waves did not seem to increase considerably with the applied fields. Hirshburg & Florschuetz (1982) have compiled data showing that the zero-field waves have little effect on Nusselt's heat-transfer predictions at the moderate film Reynolds numbers ($Re \lesssim 40$) encountered in our experiments.

5.2. *Heat-transfer measurements*

The average total heat-transfer coefficient was estimated to be given by

$$\bar{h}_{\mathrm{T}} = \frac{M}{2\pi R_0 L} \frac{h_{\mathrm{fg}}}{T_3 - 0.5(T_4 + T_5)}. \tag{37}$$

Here M is the total mass-condensation rate along the tube, L the tube's length and h_{fg} the liquid's enthalpy of evaporation. The location of the temperatures used is given in figure 5. The wall of the condensation tube offers a significant resistance. Estimating that the tube-wall heat-transfer coefficient h_{w} is 769 W/m^2 K (using the glass's thermal conductivity $k_{\mathrm{p}} = 1.17$ W/m K and the wall thickness), we obtain an estimate of the average film coefficient

$$\bar{h} = \frac{1}{1/\bar{h}_{\mathrm{T}} - 1/h_{\mathrm{w}}}. \tag{38}$$

We have neglected the resistance to heat transfer on the cold-water side, but we judge it to be small. In addition, the experimental setup does not justify a more accurate model. (The principal objective behind the glass test section was visualization of the phenomenon.) Thus we are satisfied with the estimate of the heat-transfer coefficient provided by (38).

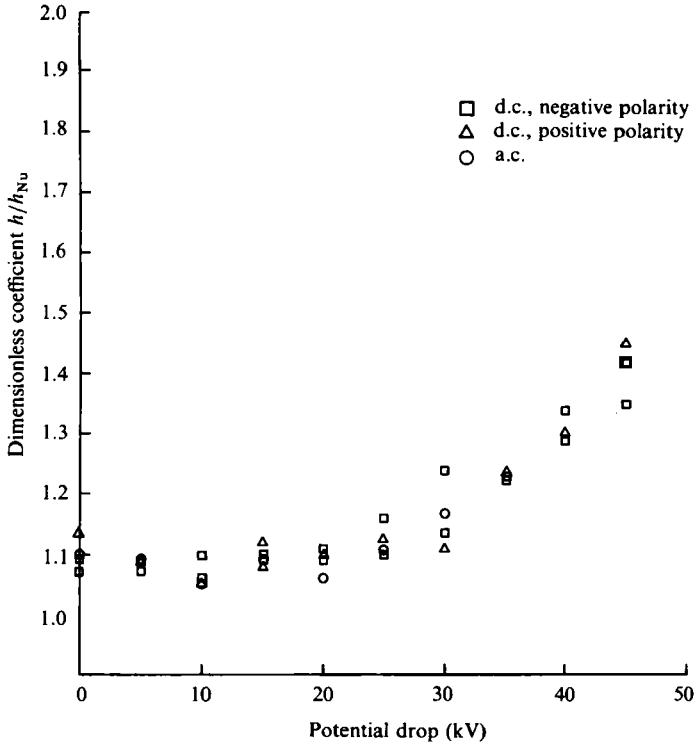

FIGURE 7. Experimental average heat-transfer measurements – concentric case.

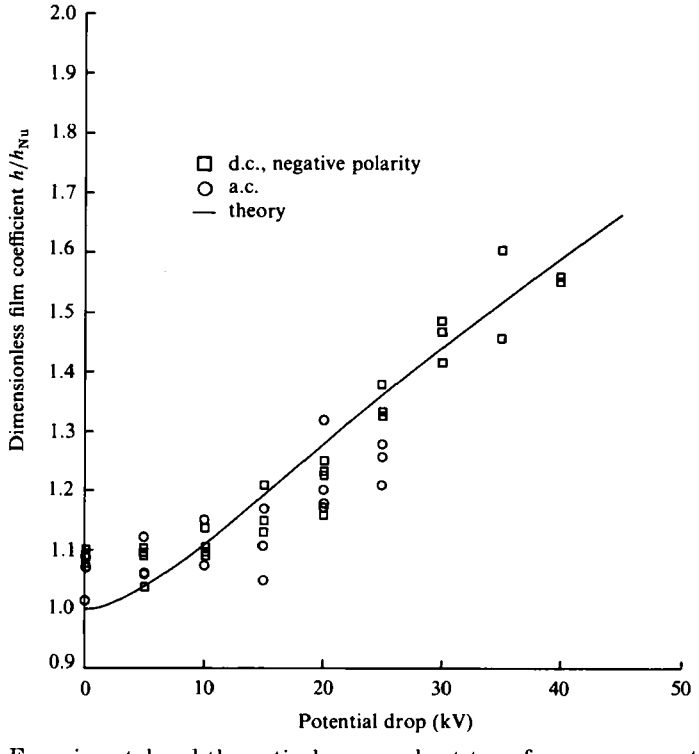

FIGURE 8. Experimental and theoretical average heat-transfer measurements – eccentric case.

Figures 7 and 8 show the average heat-transfer coefficient obtained from (38) normalized by the corresponding calculated average heat-transfer coefficient for the zero-field (Nusselt) case in terms of the imposed voltage drop. The increase in the heat-transfer coefficient with voltage drop in figure 6, where the inner electrode is centred, is due to the cusped-wave instability discussed earlier. The significant increase in heat transfer coincides with the voltages at which these waves appeared. The increase in heat transfer for the eccentric electrode is explained satisfactorily by predictions from the model presented. Comparing the results for the two positions of the electrode, it is evident that the non-uniformity of the electrical field contributes significantly to the heat-transfer rate, the increases in heat transfer occurring at lower applied voltages than those required to produce improvements in the axisymmetric case. The effect cannot be explained by the production of cusped waves, as these occur in the thickest region of the film. Thus the mechanism involved must be that of 'pulling' the liquid to one side. We do not state, however, that this mechanism will always prevail; it is quite possible that at even higher field strengths wave instabilities will dominate.

Note finally that the difference in measured average heat transfer for applied a.c. and d.c. voltage is within the experimental error of our measurements, thus confirming again that the effects of net free charge at the liquid–vapour interface are negligible.

6. Summary

We have studied film-condensation heat transfer in the presence of non-uniform electrostatic fields. A model was developed for thin films, accounting for electrical forces on the film and neglecting waviness and instability problems. We ran two experiments in one apparatus with different electrode configurations. One was designed to exploit the mechanism the model considers ('pulling' of the surface to one side); the other did not. The model compared well with the former experiment both visually and from heat-transfer considerations. Comparison of the two experiments demonstrated that the mechanism we proposed actually predominated over the others involved; namely instabilities and waviness.

Mr I. C. Kinsale designed, constructed and made preliminary runs with the experimental apparatus. Messrs E. Landry and N. A. Johnson gave us technical support in the laboratory. Dr N. Abuaf advised us on certain experimental issues.

REFERENCES

Choi, H. Y. 1968 *Trans. ASME* C: *J. Heat Transfer* **90**, 98.

Churchill, R. V., Brown, J. W. & Verhey, R. F. 1974 *Complex Variables and Applications*, 2nd edn, p. 319. McGraw-Hill.

Didkovsky, A. B. & Bologa, M. K. 1981 *Intl J. Heat Mass Transfer* **24**, 811.

Dyakowski, T., Trommelmans, J. & Berghmans, J. 1982 In *Proc. 7th Intl Heat Transfer Conf., Munich*, vol. 5, p. 65. McGraw-Hill.

Hirshburg, R. I. & Florschuetz, L. W. 1982 *Trans. ASME* C: *J. Heat Transfer* **104**, 152.

Holmes, R. E. & Chapman, A. J. 1970 *Trans. ASME* C: *J. Heat Transfer* **92**, 616.

Jones, T. B. 1978 In *Advances in Heat Transfer* (ed. T. F. Irvine & J. P. Hartnett), p. 110. Academic.

LANDAU, L. D. & LIFSHITZ, E. M. 1960 *Electrodynamics of Continuous Media*, pp. 67, 68. Pergamon.

PANOFSKY, W. K. H. & PHILLIPS, M. 1962 *Classical Electricity and Magnetism*, 2nd edn, pp. 111–113. Addison-Wesley.

ROHSENOW, W. M. 1956 *Trans. ASME* **78**, 1645.

TROMMELMANS, J. & BERGHMANS, J. 1982 *ASME Publ.* 82-WA/HT-19.

VELKOFF, H. R. & MILLER, J. H. 1965 *Trans. ASME* C: *J. Heat Transfer* **87**, 197.

YABE, A., KIKUCHI, K. & TAKETONI, T. 1982 In *Proc. 7th Intl Heat Transfer Conf., Munich*, vol. 5, p. 189. McGraw-Hill.